PAUL SCHERRER INSTITUT

Record

TM-44-25-04

Title

PSI/Nagra TDB, effect of temperature and pressure:
II. Updated selection of temperature dependent parameters of solids and aqueous complexes in the system Fe, Al, Si, Ca, Mg, SO_4^{2-}, CO_3^{2-}, PO_4^{2-}.

Author(s) / Coauthor(s)

George Dan Miron

Composed
04.07.2025, MG44

Classification NOT CLASSIFIED

Subject:

In this report the updated selection of thermodynamic properties for major solids and aqueous complexes in the system Fe, Al, Si, Ca, Mg, SO_4^{2-}, CO_3^{2-}, PO_4^{2-} is detailed. This is part of the ongoing update of the PSI/Nagra database for improved temperature (and pressure) dependencies.

Keywords:

Author:	Signature:	Date:	Reviewer:	Signature:	Date:
MG44		04.07.2025	PO44		24.08.2024

Distributor

Dep.	Addresses	Cop.	Dep.	Addresses	Cop.
4400	S. Churakov	1*	Nagra	R. Wüst	1*
4403	N. Prasianakis	1*			
4403	G. D. Miron	1*		* electronic copy	
4406	J. Provis	1*			
	TM-Dossier (Sekretariat)	1*			

	Cop.
Archiv LES	1*
Pages	35
Attachments	
Signature Head of Dep.:	

VOLES05

Version Updates

Revision	Date	Modification
1.0	04.07.2025	First draft
2.0	03.09.2025	Fixes after review by PO44
2.1	01.11.2025	Fixes after review by PO44
2.2	05.01.2026	Fixes of Al phases, removed garnets, added selection for wollastonite

Contents

0 Terms, definitions, and standards 4
0.1 Terms and abbreviations....4
1 Introduction 6
2 Selection for minerals....9
3 Selection for aqueous species 23
4 References....31

0 Terms, definitions, and standards

Selected thermodynamic data refer to the reference temperature $T_r°$ of 298.15 K (25 °C) and to the standard state, i.e., a reference pressure $P_r°$ of 0.1 MPa (1 bar), for aqueous species, infinite dilution (I = 0), for gases, ideal gas and pure solids and water solvent.

0.1 Terms and abbreviations

$\log_{10}K°$	logarithm (base-10) of the equilibrium constant of a reaction
$\log_{10}K_s°$	logarithm (base-10) of the solubility product
$\Delta_r G_m°$	molar Gibbs free energy of reaction (kJ · mol^{-1})
$\Delta_r H_m°$	molar enthalpy of reaction (kJ · mol^{-1})
$\Delta_r S_m°$	molar entropy of reaction (J · K^{-1} · mol^{-1})
$\Delta_r C_{p,m}°$	molar heat capacity of reaction (J · K^{-1} · mol^{-1})
$\Delta_r V_m°$	molar volume of reaction (g · cm^{-3})
$\Delta_f G_m°$	standard partial molar Gibbs free energy of formation (kJ · mol^{-1})
$\Delta_f H_m°$	standard partial molar enthalpy of formation (kJ · mol^{-1})
$\Delta_f S_m°$	standard partial molar entropy of formation (J · K^{-1} · mol^{-1})
$\Delta_f C_{p,m}°$	standard partial molar heat capacity of formation (J · K^{-1} · mol^{-1})
$S_m°$	standard partial molar entropy (J · K^{-1} · mol^{-1})
$C_{p,m}°$	standard partial molar heat capacity (J · K^{-1} · mol^{-1})
$V_m°$	standard partial molar volume (cm^3 mol^{-1})
Ξ_m°	standard partial molar property
$T_r°$	reference temperature of 298.15 K (25 °C)
$P_r°$	reference pressure of 1·10^5 Pa (1 bar)
M	molarity (mol · L^{-1} solution)
m	molality (mol · kg^{-1} H_2O)

I	ionic strength (mol · kg^{-1} H_2O)
P_{sat}	water saturated vapor pressure
TDB 2020	update to the PSI/Nagra chemical thermodynamic database (Hummel and Thoenen, 2023)
SIT	specific ion interaction theory aqueous activity model
HKF	Helgeson-Kirkham-Flowers model

1 Introduction

"*The text of this section is derived from Miron (2024a), expanded and revised for use here*".

The PSI/Nagra Thermodynamic database project supports the ongoing safety assessments for the planned repositories for low- and intermediate-level (L/ILW) and high-level (HLW) radioactive waste in Switzerland. The database was updated in version TDB 2020 (Hummel and Thoenen, 2023). The TDB 2020 includes thermodynamic data for 53 elements and their aqueous species, solids and gases.

Early versions of the PSI/Nagra chemical thermodynamic database (Hummel et al., 2002) focused on selecting thermodynamic properties for compounds and product species described in reactions from master species at reference temperature (T_r 298.15 K) and pressure (P_r $1 \cdot 10^5$ Pa or 1 bar). Such data are used for chemical thermodynamic calculations with the law of mass action algorithm based on the equilibrium constant ($\log_{10}K°$). Values of reaction constants for all involved aqueous product species, solids, and gases and represents are included. This represents the minimal dataset required for calculating chemical equilibria at 1 bar and 25˚C, whereas no thermodynamic data are required for the master species.

The TDB 2020 (Hummel and Thoenen, 2023) update of the PSI/Nagra chemical thermodynamic database considered the effect of temperature on the thermodynamic properties of aqueous species when selecting reference thermodynamic data. When sufficient experimental data at various temperatures were available, they were used in Hummel and Thoenen (2023) to determine values for the standard molar reaction enthalpy ($\Delta_r H_m°$) or entropy ($\Delta_r S_m°$) and heat capacity ($\Delta_r C_{p,m}°$). A complete set of $\Delta_r H_m°$ values and sometimes also $\Delta_r C_{p,m}°$ was retrieved for compounds and complexes involving Li, Na, K, Mg, Ca, Sr, Ba, Ra, Mn, Al, Fe, and Si elements, and aqueous complexes with OH^-, F^-, HCO_3^-, CO_3^{2-}, and SO_4^{2-}.

A comprehensive thermodynamic database contains not only reaction properties, but also thermodynamic properties of individual master and product species, and the parameters needed to make temperature and pressure corrections. Such an extensive database provides the means to maintain formal thermodynamic consistency between properties of substances and reactions, and extends the ranges of validity for geochemical calculations.

To use a thermodynamic database in GEM (Gibbs energy minimisation) codes (e.g., GEM-Selektor (Kulik et al., 2013)) it must include the standard molar Gibbs energy ($\Delta_f G_m°$) of all substances. These are related to the reaction constant by:

$$\log_{10}K° = \Delta_r G_m° \cdot [R \cdot T° \cdot \ln(10)]^{-1} \qquad 1\text{-}1$$

For calculations at conditions different from T_r and P_r, the $\Delta_f G_m°$ values need to be corrected to the temperature and pressure of interest. For this, data on standard molar entropy ($S_m°$) or enthalpy ($\Delta_f H_m°$), heat capacity ($C_{p,m}°$), and volume ($V_m°$) at T_r and P_r, and data on their temperature and pressure dependencies, are required for each individual species in the chemical system.

Provided information on $S_m°$ or $\Delta_f H_m°$, and $C_{p,m}°$, at T_r and P_r of master species, the $S_m°$ or $\Delta_f H_m°$, and $C_{p,m}°$, of all dependent substances can be calculated from their respective reaction partial molar properties ($\Delta_r \Xi_m^\circ$):

$$\Delta_r \Xi_m^\circ = \sum_{i=1}^{n} \nu_i \cdot \Xi_{m,i}^\circ \qquad 1\text{-}2$$

where Ξ_m° is a partial molar property of a species i, and ν_i represents the stoichiometric coefficients, negative for reactants and positive for products.

In addition to values for $\Delta_f G_m°$, the TDB 2020 contains values for $S_m°$ or $\Delta_f H_m°$ for most master species, while most do not have $C_{p,m}°$ values. No $V_m°$ data were evaluated for any of the compounds selected in the TDB 2020 or in any previous PSI-Nagra database releases.

The missing $S_m°$ or $\Delta_f H_m°$, $C_{p,m}°$, and $V_m°$ values, and lack of data on their temperature and pressure dependency, prevents use of the database for calculations at conditions other than at T_r and P_r. Additionally, data on $V_m°$ of solids are necessary for using the database in reactive transport model calculations where changes in porosity due to mineral dissolution/precipitation are important. For improved modelling calculations applied to deep geological repositories, a consistent and complete set of thermodynamic properties of substances and reactions, including molar volumes as well as their temperature (pressure) dependence, is necessary. (Miron, 2024a)

The extension of the TDB 2020 to include a complete set of thermodynamic properties for temperature (and pressure) changes started in part I of the effect of temperature and pressure series with selecting the properties for master species and selected dependent species containing H, O, P, C, S, Cl, F, Na, K, Mg, Ca, Al, Fe, and Si elements, molar volumes for solid phases, and heat capacity data for gases in TDB 2020 (Miron, 2024a).

In this report, the selection continues with selecting missing or revising values for $S_m°$ or $\Delta_f H_m°$, $C_{p,m}°$, and $V_m°$ and respective reaction properties of selected major rock forming solids, oxides, hydroxides, sulphates, silicates, and relevant hydrolysis species (Fe, Al) in the system Fe, Al, Si, Ca, SO_4^{2-}, CO_3^{2-} as well as data for the $H_2PO_4^-$ and H_3PO_4(aq) species. The selection is based on CODATA (Cox et al., 1989), the updated NEA Ancillary data (Rand et al., 2024), the TDB2020 data evaluation (Hummel and Thoenen, 2023), the review of Robie and Hemingway (1995), and the work of Brown and Ekberg (2016). The starting values are taken from Rand et al. (2024) or TDB2020. The data are selected from the original source, or are re-evaluated based on the following criteria: agreement with solubility and calorimetry data – the retrieved properties should reproduce the evaluated solubility or formation constants data (using the SIT (Specific ion Interaction Theory) model (Guggenheim and Turgeon, 1955) as well as be in agreement with the properties of solids derived from calorimetry.

The data will be made available in GEMS and in PHREEQC formats in the upcoming electronic releases. The validity of the selected data is at least within the range 0-150 ℃ and P_{sat}-300 bar. For gases, the ideal gas model is used, which does not produce significant deviations below 50 bar.

The aim of future work is the compilation of a complete set of thermodynamic properties for all compounds to complement the reaction properties in the PSI/Nagra database, in order to optimise temperature and pressure extrapolations. Hence, further updates as well as continuous improvement based on new experimental data and improved understanding of these systems are critical.

Future updates should also include selections of data for other pore water elements (e.g., Li, Ba, Ra, Sr, Mn), and missing properties and HKF model parameters for all master specie including radionuclides ions. Data on heat capacity as a function of temperature for solid phases based on calorimetric measurements should also be selected and their consistency with derived values at T_r and P_r, based on solubility data in TDB 2020 where available, should be assessed. For gas solubility, SIT aqueous activity model (Guggenheim and Turgeon, 1955) parameters need to be evaluated. Finally, the available temperature data on the aqueous complexation (hydrolysis, chlorine, fluorine, carbonate, sulphate, phosphate, nitrate, and silicate) of radionuclides needs to be assessed and a set of missing properties for these would be generated based on analogies, linear energy and ionic radius relationships, and the use of isocoulombic reactions.

The selected data in this report are consistent with the SIT model and parameters evaluated in TDB 2020. (Miron, 2024a)

2 Selection for minerals

In addition to values for $C_{p,m}°(298.15\ K)$, for solids, where available, coefficients of the $C_{p,m}°(T)$ function were also selected and are provided in Table 3-1.

α-SiO_2(cr) (quartz)

Properties from CODATA (Cox et al., 1989) as in TDB 2020 (Hummel and Thoenen, 2023).

Aluminium

α-Al_2O_3(cr) (corundum)

Properties from CODATA (Cox et al., 1989) as in TDB 2020 (Hummel and Thoenen, 2023).

Major aluminum hydroxide compounds have the formulas $Al(OH)_3$ and AlOOH, these are named Al tryhidroxides and Al oxyhydroxides or alumina trihydrate and monohydrate (Hsu, 1989). The important polymorphs identified in natural systems (e.g., bauxite deposits) are gibbsite (γ-alumina trihydrate), bayerite (α-alumina trihydrate), boehmite (γ-alumina monohydrate), and diaspore (α-alumina monohydrate). These phases are also important in the engineered systems such as the Bayer process that is used to extract Al. This process involves high temperatures, pressures, NaOH solutions and subsequent seeded gibbsite precipitation at lower temperatures (~50 °C).

$Al(OH)_3$(cr) (gibbsite)

Thermodynamic properties of gibbsite (γ-aluminium hydroxide) were used as anchor to derive a consistent set of standard thermodynamic properties (at I = 0) for solids and aqueous species in the system Al–O–H (Miron, 2024b). Values for $\Delta_f H_m°$, $\Delta_f S_m°$, and $\Delta_f C_{p,m}°$ of gibbsite were taken from Robie and Hemingway (1995) and were based on thermochemical measurements of (Hemingway et al., 1977; Hemingway and Robie, 1977). These values are the same as those selected in the NEA TDB (Rand et al., 2024) with the exception of the enthalpy of -1294.0 ±1.5 kJ·mol^{-1} in NEA.

$$\Delta_f H_m°(298.15\ K) = \mathbf{-(1293.130 \pm 1.19)}\ kJ{\cdot}mol^{-1}$$

$$S_{abs}°(298.15\ K) = \mathbf{68.44 \pm 0.3}\ J{\cdot}K^{-1}{\cdot}mol^{-1}$$

$$C_{p,m}°(298.15\ K) = \mathbf{91.72 \pm 0.3}\ J{\cdot}K^{-1}{\cdot}mol^{-1}$$

Selected properties of the Al^{3+} ion (Miron, 2024a) were then calculated based on the gibbsite solubility reaction properties derived in the review of Brown and Ekberg (2016). The properties for this reaction are the same properties selected in TDB 2020:

$$Al(OH)_3(cr)\ (gibbsite) + 3\ H^+ = Al^{3+} + 3\ H_2O(l) \qquad 2\text{-}1$$

$$\log_{10}K_s°(298.15\ K) = \mathbf{7.75 \pm 0.08}$$

$$\Delta_r H_m°(298.15\ K) = \mathbf{-(104.3 \pm 2.3)}\ kJ{\cdot}mol^{-1}$$

$$\Delta_r C_{p,m}°(298.15\ K) = \mathbf{0}\ J{\cdot}K^{1}{\cdot}mol^{-1}$$

In cementitious systems more soluble amorphous and microcrystalline aluminium hydroxide phases have been identified (Lothenbach et al., 2022, 2012). These phases are metastable with respect to gibbsite, have a similar XRD patter with border peaks. Their solubility decreases with time. For using them in scoping calculations or modelling metastable states the following supplemental data for $Al(OH)_3$(mcr) are selected from the measurements of (Lothenbach et al., 2012) which show an almost constant solubility constant from 0 to 60 °C at 19 months. (Lothenbach et al., 2022) provide data on the enthalpy of formation of Al(OH)3(mcr). These combined with the $\log_{10}K_s°(298.15\ K)$ *–(0.67 ± 0.2*) and the properties of the OH- and Al(OH)4- are used to derive the Gibbs energy and entropy of this phase. The heat capacity is estimated as $1.1{\cdot}S_{abs}°$ (Lothenbach et al., 2022) and the volume is taken from (Lothenbach et al., 2022).

$$Al(OH)_3(mcr) + OH^- = Al(OH)4^- \qquad 2\text{-}2$$

$$\log_{10}K_s°(298.15\ K) = \textit{-(0.67 ± 0.3)}$$

The following thermodynamic properties of $Al(OH)_3$(mcr) are selected

$$\Delta_f G_m°(298.15\ K) = \textit{-(1152.4 ± 2.0)}\ kJ{\cdot}mol^{-1}$$

$$\Delta_f H_m°(298.15\ K) = \textit{-(1275.9 ± 3.5)}\ kJ{\cdot}mol^{-1}$$

$$S_{abs}°(298.15\ K) = \textit{117.74 ± 13}\ J{\cdot}K^{-1}{\cdot}mol^{-1}$$

$$C_{p,m}°(298.15\ K) = \textit{130 ± 14}\ J{\cdot}K^{-1}{\cdot}mol^{-1}$$

$$\textit{V_m°(298.15 K) = 38.04 cm^3}$$

This phase should only be used when modeling systems < 70 °C and requires additional independent confirmation to accompany modeling predictions. Above 70 °C gibbsite should be used instead, unless there are independent reasons to use microcrystalline gibbsite instead.

$Al(OH)_3$(s) (bayerite)

Bayerite (α alumina trihydrate) is a polymorph of Al hydroxide ($Al(OH)_3$) (others being nordstrandite and doyleite), a metastable phase between amorphous $Al(OH)_3{\cdot}nH_2O$ and gibbsite. During precipitation from aluminium rich solutions, particularly under alkaline

solutions, the formed solids evolve through intermediate amorphous to crystalline phases (i.e., an ageing process), bayerite being preferred by fast precipitation kinetics (Zhang et al., 2021) from highly supersaturated soda rich solutions. No data for bayerite were selected in previous TDB updates. Bayerite could form in alkali activated aluminium rich systems, and the phase is relevant for processing of aluminum ore (bauxite), and caustic nuclear waste (Zhang et al., 2021). The available solubility and calorimetric data for bayerite were recently reviewed by Rand et al. (2024). Based on their evaluation the following properties were selected:

$$\Delta_f H_m^\circ(298.15\ \mathrm{K}) = \mathbf{-(1289.0 \pm 2.5)}\ \mathrm{kJ\cdot mol^{-1}}$$

$$Al(OH)_3(s) + OH^- = Al(OH)_4^- \qquad 2\text{-}3$$

$$\log_{10} K_s^\circ(298.15\ \mathrm{K}) = \mathbf{-(0.871 \pm 0.026)}$$

For a complete set of properties, the value of $C_{p,m}^\circ(298.15\ \mathrm{K})$ is approximated by assuming the same difference to gibbsite as the one obtained for the entropy of +9 $\mathrm{J\cdot K^{-1}\cdot mol^{-1}}$. This is also consistent with $1.1\cdot S_{abs}^\circ$ approximation. The molar volume for this phase, *33.18* $\mathrm{cm^3}$, is estimated by adding to the volume of gibbsite a volume correction obtained using the entropy volume relation (Glasser and Jenkins, 2016) on the difference between the entropies of gibbsite and bayerite.

Using the above values and properties of reactants from Miron (2024a), the selected reaction (2-3) properties are:

$$\log_{10} K_s^\circ(298.15\ \mathrm{K}) = \mathbf{-(0.871 \pm 0.026)}$$

$$\Delta_r H_m^\circ(298.15\ \mathrm{K}) = \mathbf{16.2 \pm 2.5}\ \mathrm{kJ\cdot mol^{-1}}$$

$$\Delta_r C_{p,m}^\circ(298.15\ \mathrm{K}) = \mathbf{212}\ \mathrm{J\cdot K^{1}\cdot mol^{-1}}$$

The selected properties of bayerite are:

$$\Delta_f H_m^\circ(298.15\ \mathrm{K}) = \mathbf{-(1289.0 \pm 2.5)}\ \mathrm{kJ\cdot mol^{-1}}$$

$$S_{abs}^\circ(298.15\ \mathrm{K})^* = \mathbf{77.649 \pm 10}\ \mathrm{J\cdot K^{-1}\cdot mol^{-1}}$$

$$C_{p,m}^\circ(298.15\ \mathrm{K}) = \mathbf{100.7 \pm 10}\ \mathrm{J\cdot K^{-1}\cdot mol^{-1}}$$

*calculated from reaction 2-3 properties and reactants data from Miron (2024a)

The resulted entropy of bayerite is higher than that of gibbsite which is consistent if we assume that beyerite is more hydrated, disordered phase.

When comparing the reaction constant at different temperatures calculated based on the selected data, the agreement is good (Figure 2-1). Even though no heat capacity was selected by Rand et al. (2024) its effect on the reaction constant is small in the temperature range of 0-100 °C. Based on the selected thermodynamic data, bayerite is metastable with respect to gibbsite from ambient to high temperatures. Its formation may be related to supersaturated high alkaline and fast crystallization systems.

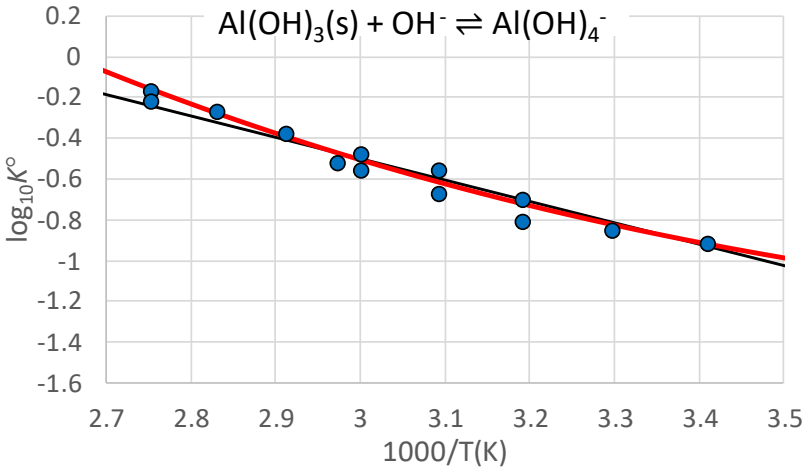

Figure 2-1: $\log_{10}K°(T)$ of bayerite solubility reaction (2-3) calculated based on the selected data (red line) and based on data from Rand et al. (2024) (black line), compared with experiments evaluated in Rand et al. (2024) (blue points).

Al(OOH)(cr) (boehmite)

Thermodynamic properties of boehmite (γ-Al(OOH)(cr)) were evaluated in TDB 2020 (Hummel and Thoenen, 2023). These were derived from a fit to solubility data at different temperatures that included two data points at 70 and 90 ℃ from (Verdes et al., 1992). The two points break the linear trend of the other high temperature solubility measurements (Figure 2-2).

When deriving the standard properties of boehmite from the reaction properties, a low value for $C_{p,m}°$(298.15 K) of 16.2 J·K^{1}·mol^{-1} and a value of -963.10 for the enthalpy of formation. These are deviating from the values obtained from calorimetry of -996.1 ±1.3 (Chen and Zeng, 1996), 54.24 J·K^{1}·mol^{-1} for for $C_{p,m}°$ (Hemingway et al., 1991). An alternative fit can be obtained if the two datapoints are ignored, only the measurements >100 ℃ are considered and the $C_{p,m}°$ of boehmite is constrained to 54.24 J·K^{1}·mol^{-1} (Hemingway et al., 1991). The following reaction properties are then derived:

$$AlOOH(cr) + 3H^+ = Al^{3+} + 2H_2O(l) \qquad 2\text{-}4$$

$$\log_{10}K_s°(298.15\ K) = \mathbf{7.61 \pm 0.5}$$

$$\Delta_r H_m°(298.15\ K) = \mathbf{-(115.5 \pm 2.3)}\ kJ·mol^{-1}$$

$$\Delta_r C_{p,m}°(298.15\ K) = \mathbf{-38 \pm 40}\ J·K^{1}·mol^{-1}$$

From the derived reaction properties the following thermodynamic properties of boehmite are obtained

$$\Delta_f G_m°(298.15\ K) = \mathbf{-(918.58 \pm 2.5)}\ kJ·mol^{-1}$$

$\Delta_f H_m°(298.15\ K) = \mathbf{-(996.1 \pm 2.5)}$ kJ·mol^{-1}

$S_{abs}°(298.15\ K) = \mathbf{38.8 \pm 3}$ J·K^{-1}·mol^{-1}

These values are in good agreement with those of $\Delta_f H_m°$ (Chen and Zeng, 1996) and $S_{abs}°$ of (Hemingway et al., 1991) of 37.17.

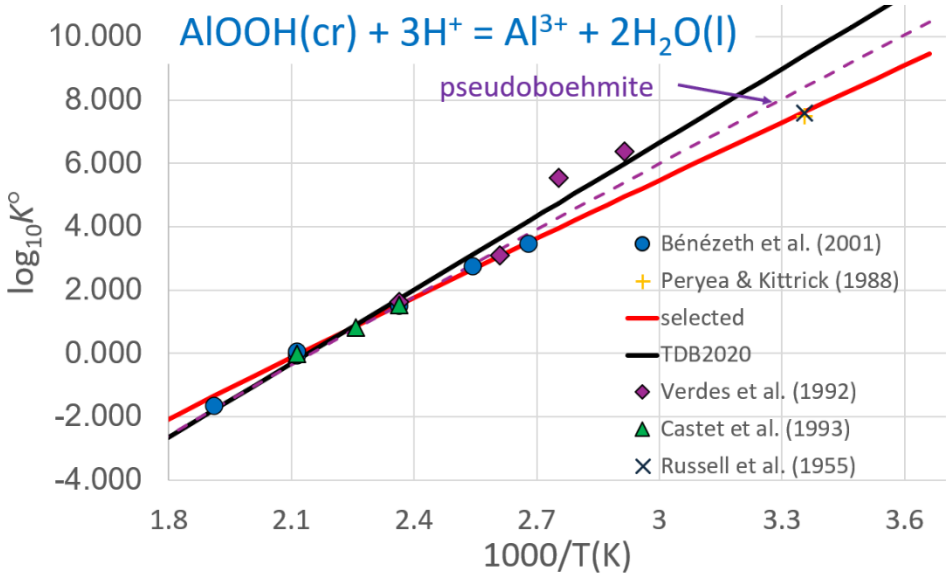

Figure 2-2: $\log_{10}K°(T)$ of the solubility of boehmite **Error! Reference source not found.** compared to measured data (Bénézeth et al., 2001; Peryea and Kittrick, 1988; Russell et al., 1955; Verdes et al., 1992). Data form (Peryea and Kittrick, 1988; Russell et al., 1955) are estimates from high temperature measurements. Dashed line is calculated based on supplemental data for AlOOH(mcr) (pseudoboehmite), red line is based on selected data for crystalline boehmite.

When considering the bulk thermodynamic properties of gibbsite and boehmite, boehmite is predicted to be the more stable phase above 5 ℃. This seems to be in disagreement with observations that gibbsite does not convert to boehmite <80 ℃ even after months (Palmer and Wesolowski, 1992; Wesolowski, 1992) and that boehmite synthesis employs hydrothermal conditions > 90 ℃ (Shin et al., 2020; Skoufadis et al., 2003). (Chen et al., 2018) suggest that the transformation of gibbsite to boehmite may happen through dissolution of gibbsite and crystallization of boehmite while (Panasyuk et al., 2010) propose a solid – state transformation in their hydrothermal experiments. (Skoufadis et al., 2003) in their kinetic analysis in highly alkaline solutions propose that boehmite has a large activation energy for its precipitation reaction which makes it kinetically favoured only at high temperatures, while gibbsite is favoured at low and ambient temperatures. (Russell et al., 1955) based on extensive measurements of the solubility of aluminium hydroxides in NaOH solutions concluded that hydrothermally synthesized boehmite is more stable than gibbsite above 26 ℃ in pure water. The author noticed that boehmite freshly precipitated transforms to gibbsite in alkaline solution at room temperature while boehmite produced hydrothermally does not. The hydrothermal boehmite would then be the phase consistent with the bulk

thermodynamic properties of boehmite, while the precipitated boehmite would be a metastable phase more soluble than gibbsite.

Observations of aluminium phases in soils and bauxites suggest that close to ambient conditions and close to neutral pH, “boehmite” would precipitate as a gel like, microcrystalline phase (Hsu, 1989). This would be a more soluble phase than the hydrothermal crystalline boehmite that by ageing would convert to gibbsite or in dry conditions to a more crystalline boehmite. Gibbsite microcrystalline phases are observed in alkaline aluminate cement systems (Lothenbach et al., 2012).

Various effects such as crystal size, surface, pH, presence of other ions, supersaturation, water activity, lead to several metastable states concerning the gibbsite and boehmite stability at the earth surface and ambient temperatures (Majzlan et al., 2000; Trolard and Tardy, 1987). Accounting for the additional uncertainties that exist in their the thermodynamic properties this makes it difficult to predict the stable phase based only on bulk thermodynamics. Based on experimental observations (Chesworth, 1972) suggest that gibbsite+boehmite assemblages may be stable at ambient conditions. Boehmite is stabilized with decreasing water activity and increasing temperature (Trolard and Tardy, 1987).

Additional supplemental data is provided for “pseudobohemite” (AlOOH(mcr)) derived from the unweighted fit all points in Figure 2-2, including from (Verdes et al., 1992), with the constraint of having positive $C_{p,m}^\circ = 1.1 \cdot S_{abs}^\circ$ and S_{abs}° larger than those of boehmite (crystalline, hydrothermal). The following properties are obtained:

$$AlOOH(mcr) + 3H^+ = Al^{3+} + 2H_2O(l) \qquad 2\text{-}5$$

$$\log_{10}K_s^\circ(298.15\ K) = 8.4 \pm 1.0$$

$$\Delta_r H_m^\circ(298.15\ K) = -(129.3 \pm 6)\ kJ\cdot mol^{-1}$$

$$\Delta_r C_{p,m}^\circ(298.15\ K) = -(60.8 \pm 20)\ J\cdot K^{1}\cdot mol^{-1}$$

From the derived reaction properties the following supplemental thermodynamic properties of AlOOH(mcr) are obtained

$$\Delta_f G_m^\circ(298.15\ K) = -(914.1 \pm 6)\ kJ\cdot mol^{-1}$$

$$\Delta_f H_m^\circ(298.15\ K) = -(982.3 \pm 6)\ kJ\cdot mol^{-1}$$

$$S_{abs}^\circ(298.15\ K) = 70 \pm 15\ J\cdot K^{-1}\cdot mol^{-1}$$

$$C_{p,m}^\circ(298.15\ K) = 77 \pm 20\ J\cdot K^{-1}\cdot mol^{-1}$$

The molar volume for this phase, *29.15* cm^3, is estimated by adding to the volume of boehmite a volume correction obtained using the entropy volume relation (Glasser and Jenkins, 2016) on the difference between the entropies of boehmite and microcrystalline boehmite.

This phase is provided for performing scooping calculations and modeling metastable systems and should not be used above temperatures of 100-150 °C, but boehmite should be used instead.

Al(OOH)(cr) (diaspore)

No data for diaspore (α-Al(OOH)(cr)) were selected in TDB 2020 (Hummel and Thoenen, 2023). The phase is more relevant for high temperature conditions above 150 °C. Based on the comprehensive review of Apps et al. (1989) and the reported thermodynamic data in Robie and Hemingway (1995), diaspore would be the thermodynamically the most stable phase from room to high temperature (Figure 2-3). In natural systems bayerite, gibbsite, and boehmite appear to be metastable with respect to diaspore.

Thermodynamic data for diaspore from Robie and Hemingway (1995) are selected as supplemental:

$$\Delta_f G_m°(298.15\ K) = -(922.7 \pm 2.1)\ kJ{\cdot}mol^{-1}$$

$$\Delta_f H_m°(298.15\ K) = -(1001.3 \pm 2.2)\ kJ{\cdot}mol^{-1}$$

$$S_{abs}°(298.15\ K) = 35.3 \pm 0.2\ J{\cdot}K^{-1}{\cdot}mol^{-1}$$

$$C_{p,m}°(298.15\ K) = 53.33\ J{\cdot}K^{-1}{\cdot}mol^{-1}$$

$$V_m°(298.15\ K) = 17.76\ cm^3$$

based on the properties of the reactants (Miron, 2024a) this leads to the following selected properties of reaction:

$$AlOOH(cr) + 3H^+ = Al^{3+} + 2H_2O(l) \qquad 2\text{-}6$$

$$\log_{10}K_s°(298.15\ K) = 6.888 \pm 0.43$$

$$\Delta_r H_m°(298.15\ K) = -(110.3 \pm 3.4)\ kJ{\cdot}mol^{-1}$$

$$\Delta_r C_{p,m}°(298.15\ K) = -37.128\ J{\cdot}K^{1}{\cdot}mol^{-1}$$

Stability of aluminium hydroxides

The recommended thermodynamic data correspond to bayerite, gibbsite, boehmite, and diaspore. These phases represent the expected bulk properties of well-crystallized aluminium hydroxides and oxyhydroxides. However, due to kinetic limitations, surface effects, and interactions with dissolved ions, less crystalline and more soluble phases may form in the systems under investigation.

Supplemental data are therefore provided for AlOOH(mcr) and $Al(OH)_3$(mcr). These phases should only be used in modelling when metastability is anticipated and their presence can be confirmed by an independent analytical method. Moreover, their thermodynamic properties may not accurately represent the metastable aluminium hydroxide present in a

specific system at a given equilibration time. In general, $Al(OH)_3$(mcr) is more relevant for alkaline conditions, whereas AlOOH(mcr) is more typical near neutral pH. When performing calculations at elevated temperatures the data for AlOOH(mcr) and Al(OH)3(mcr) should not be used beyond 150 and 60 °C, respectively (Figure 2-3).

(a)

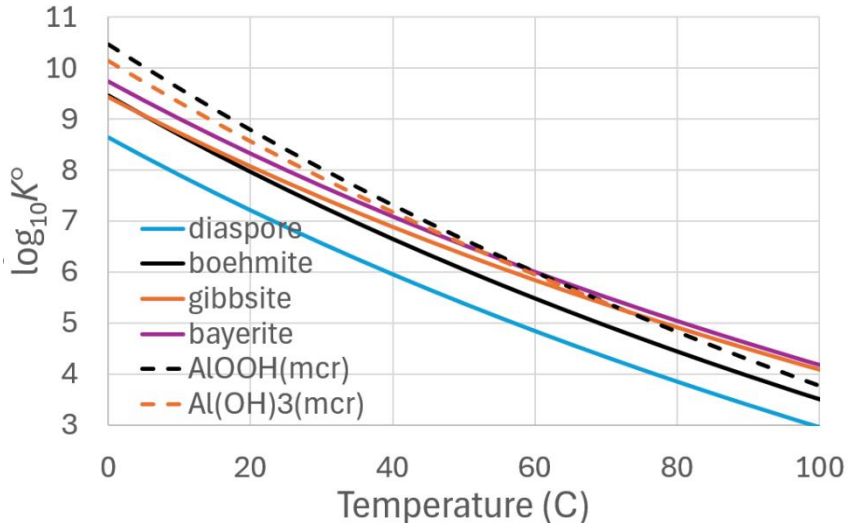

(b)

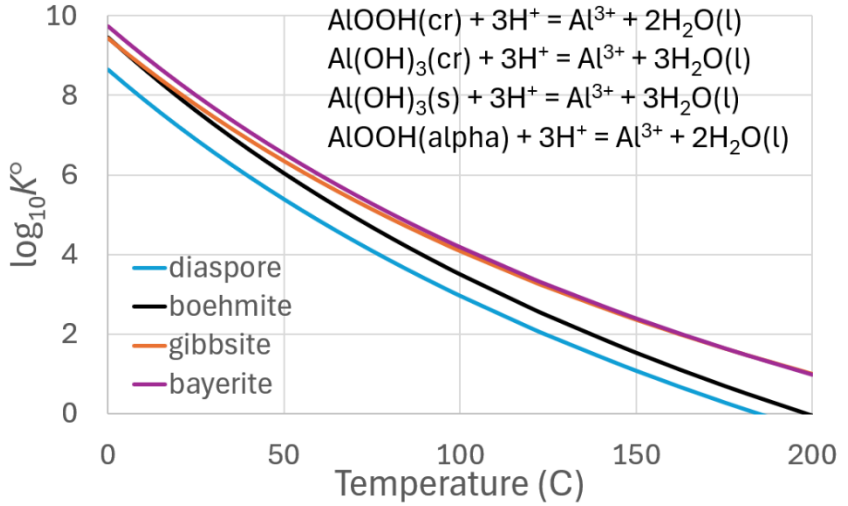

Figure 2-3: (a) Relative stability of aluminium hydroxides up to 100 °C. (b) Relative stability of boehmite ($AlOOH_{(cr)}$), gibbsite ($Al(OH)_3$(cr)), bayerite ($Al(OH)_3$(s)) and diaspore (AlOOH(alpha)). Phases with lower solubility product are less soluble.

When comparing the relative stability of the crystalline phases based on the selected thermodynamic data, diaspore is the most stable phase from ambient conditions up to high temperatures. It is followed, in order of decreasing stability, by boehmite, gibbsite, and bayerite (Figure 2-3b). In modelling applications where these phases may occur, the selection of the stable phase should always be supported by independent evidence, rather

than relying solely on thermodynamic predictions. Considering the crystalline aluminum hydroxides, gibbsite would be the primary phase close to ambient conditions, bayerite form in supersaturated fast crystallization conditions, while boehmite and diaspore are typical for hydrothermal systems.

α-Fe_3O_4(cr) (magnetite)

The selected thermodynamic properties of magnetite in TDB 2020 make the phase less soluble than based on the selected properties in Lemire et al. (2013). Data selected in TDB 2020 (Hummel and Thoenen, 2023) are:

$$1/3\ Fe_3O_4(\text{magnetite}) + 2\ H^+ + 1/3\ H_2(g) \rightleftharpoons Fe^{2+} + 4/3\ H_2O(l) \qquad 2\text{-}7$$

$$\log_{10}K_{s,0}°(298.15\ K) = 11.77 \pm 0.22$$

$$\Delta_r H_m°(298.15\ K) = -(89.4 \pm 3.4)\ kJ{\cdot}mol^{-1}$$

$$\Delta_r C_{p,m}°(298.15\ K) = 0\ J{\cdot}K^{-1}{\cdot}mol^{-1}$$

The data for the solubility reaction (2-7) in TDB 2020 were based on the review of (Brown and Ekberg, 2016), and when the retrieved reaction properties were used to calculate the standard properties of magnetite a negative heat capacity was obtained for the solid. In the reassessment by (Hummel and Thoenen, 2023) assuming $\Delta_r C_{p,m}°$ equal to zero, the obtained $C_{p,m}°$ for magnetite was 203.571 $J{\cdot}K^{-1}{\cdot}mol^{-1}$, which is 50 $J{\cdot}K^{-1}{\cdot}mol^{-1}$ larger than the value based on calorimetric measurements from Robie and Hemingway (1995).

The thermodynamic properties of magnetite reviewed by Lemire et al. (2013) are in agreement with values from calorimetric measurements reported in Robie and Hemingway (1995). These are now selected for the database:

$$\Delta_f G_m°(298.15\ K) = \mathbf{-(1012.719 \pm 1.6)}\ kJ{\cdot}mol^{-1}$$

$$\Delta_f H_m°(298.15\ K) = \mathbf{-(1115.780 \pm 1.6)}\ kJ{\cdot}mol^{-1}$$

$$C_{p,m}°(298.15\ K) = \mathbf{150.86 \pm 0.3}\ J{\cdot}K^{-1}{\cdot}mol^{-1}$$

Using these values and the properties of the reactants lead to the following updated properties of the magnetite solubility reaction:

$$\log_{10}K_s°(298.15\ K) = \mathbf{12.147 \pm 0.15}$$

$$\Delta_r H_m°(298.15\ K) = \mathbf{-(69.334 \pm 0.84)}\ kJ{\cdot}mol^{-1}$$

$$\Delta_r C_{p,m}°(298.15\ K) = \mathbf{17.58 \pm 10}\ J{\cdot}K^{1}{\cdot}mol^{-1}$$

The newly selected properties for magnetite are qualitatively indistinguishable from the previous selection in TDB2020 when compared with solubility data (Figure 2-4) but are now

consistent with values for $C_{p,m}°$ and $\Delta_f H_m°$ from calorimetric measurements (Robie and Hemingway, 1995).

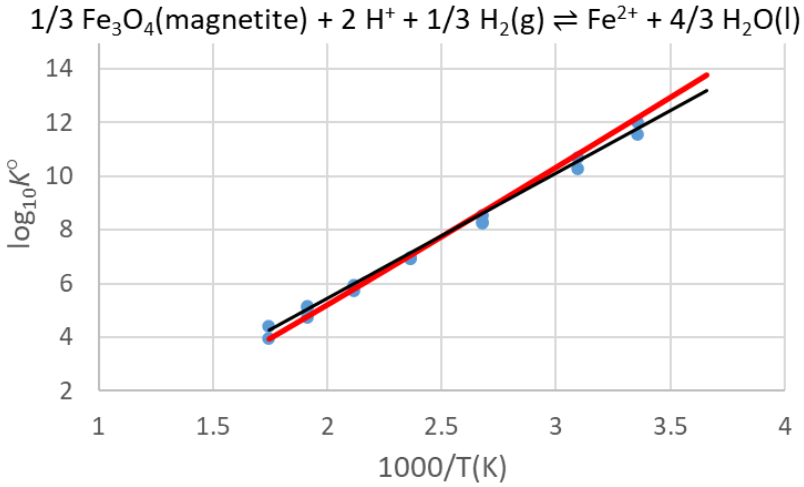

Figure 2-4: Magnetite solubility product. Blue points are experimental data compiled in Brown and Ekberg (2016); black line is TDB 2020; red line is selected properties.

α-Fe_2O_3(cr) (hematite)

The solubility product of hematite at 298.15 K selected in TDB 2020 is based on the review of Brown and Ekberg (2016).

$$1/2\ Fe_2O_3(\text{hematite}) + 3\ H^+ = Fe^{3+} + 3/2\ H_2O(l) \qquad 2\text{-}8$$

$$\log_{10}K_{s,0}°(298.15\ K) = 0.36 \pm 0.4$$

$$\Delta_r H_m°(298.15\ K) = -(68.3 \pm 1.9)\ kJ{\cdot}mol^{-1}$$

$$\Delta_r C_{p,m}°(298.15\ K) = 0\ J{\cdot}K^{-1}{\cdot}mol^{-1}$$

By assuming zero heat capacity of reaction, the resulting $\Delta_f C_{p,m}°$ of hematite would be 10.05 $J{\cdot}K^{-1}{\cdot}mol^{-1}$, which is 94 $J{\cdot}K^{-1}{\cdot}mol^{-1}$ more negative than the value in Robie and Hemingway (1995) based on calorimetric measurements. Keeping the value for the solubility product as selected in TDB 2020 and complementing this with values for $\Delta_f S_m°$, and $\Delta_f C_{p,m}°$ of hematite from Robie and Hemingway (1995) leads to the following updated selected properties for the solubility reaction:

$$\log_{10}K_{s,0}°(298.15\ K) = \mathbf{0.36 \pm 0.4}$$

$$\Delta_r H_m°(298.15\ K) = \mathbf{-(68.001 \pm 1.9)}\ kJ{\cdot}mol^{-1}$$

$$\Delta_r C_{p,m}°(298.15\ K) = \mathbf{-(46.989 \pm 20)}\ J{\cdot}K^{-1}{\cdot}mol^{-1}$$

The solubility measurements are well reproduced by the selected thermodynamic properties, while the model (Lemire et al., 2013) based only on calorimetric data leads to systematically less soluble hematite (Figure 2-5). The only difference is the solubility constant at 25 ℃. New solubility experiments on hematite at ambient and elevated temperatures might help resolve this discrepancy.

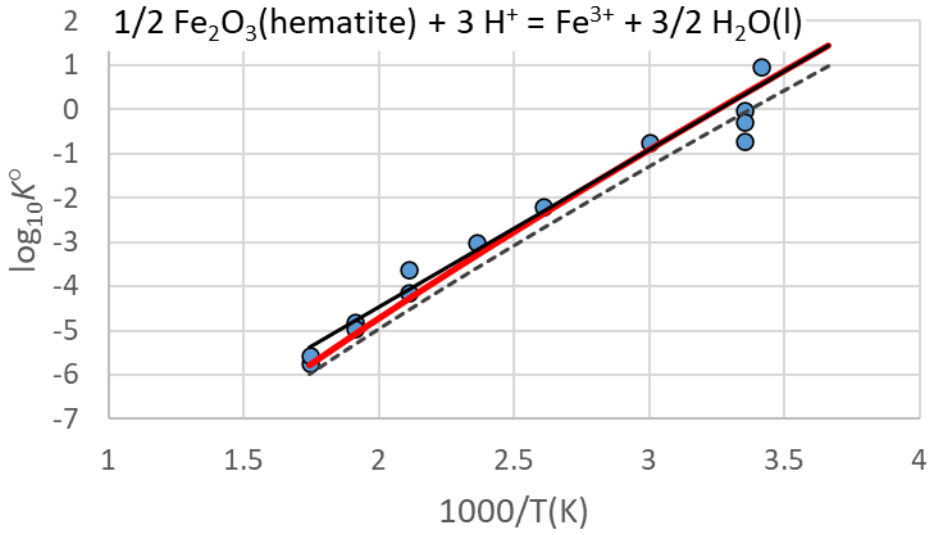

Figure 2-5: Hematite solubility product. Blue points are experimental data compiled in Brown and Ekberg (2016); black line is TDB 2020; dotted line is (Lemire et al., 2013), red line is selected properties.

α-FeOOH(cr) (goethite)

The thermodynamic data for the solubility of goethite in TDB 2020 were based on the review by Brown and Ekberg (2016).

$$FeOOH(goethite) + 3\ H^{+} = Fe^{3+} + 2\ H_2O(l) \qquad 2\text{-}9$$

$$\log_{10}K_{s,0}^{\circ}(298.15\ K) = 0.33 \pm 0.10$$

$$\Delta_r H_m^{\circ}(298.15\ K) = -(65.5 \pm 2.3)\ kJ{\cdot}mol^{-1}$$

$$\Delta_r C_{p,m}^{\circ}(298.15\ K) = 0\ J{\cdot}K^{1}{\cdot}mol^{-1}$$

Based on the linear relationship between the solubility product and the inverse of temperature, a zero heat capacity of reaction was assumed. If we take this value, the resulting $\Delta_f C_{p,m}^{\circ}$ of goethite would then be 42.7 $J{\cdot}K^{1}{\cdot}mol^{-1}$,which is lower than the value of 74.8 $J{\cdot}K^{1}{\cdot}mol^{-1}$ evaluated by Navrotsky et al. (2008) based on calorimetric measurements.

The thermodynamic properties of goethite were reviewed by Lemire et al. (2013) and are in agreement with calorimetric as well as solubility data (Figure 2-6). These values are selected and included in the database update:

$\log_{10}K_{s,0}°(298.15\ K) = \mathbf{0.17 \pm 0.34}$

$\Delta_r H_m°(298.15\ K) = \mathbf{-(65.5 \pm 2.3)}$ kJ·mol^{-1}

$\Delta_r C_{p,m}°(298.15\ K) = \mathbf{0}$ J·K^{1}·mol^{-1}

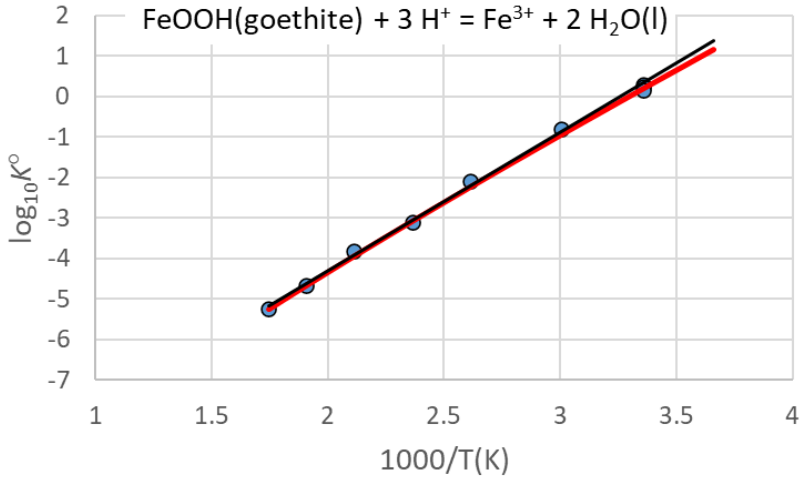

Figure 2-6: Goethite solubility product. Blue points are experimental data compiled in Brown and Ekberg (2016); black line is TDB 2020; red line is selected properties (Lemire et al., 2013).

γ-FeOOH(cr) (lepidocrocite)

The selected thermodynamic properties of magnetite were reviewed by Lemire et al. (2013) and accepted in TDB 2020. The $\Delta_r C_{p,m}°$ was omitted in TDB 2020 and is updated here

$$FeOOH(lepidocrocite) + 3\ H^+ = Fe^{3+} + 2\ H_2O(l) \qquad 2\text{-}10$$

$\log_{10}K_{s,0}°(298.15\ K) = \mathbf{1.861 \pm 0.37}$ (differences due to rounding)

$\Delta_r H_m°(298.15\ K) = \mathbf{-(72.5 \pm 2.2)}$ kJ·mol^{-1}

$\Delta_r C_{p,m}°(298.15\ K) = \mathbf{-(26.42 \pm 20.3)}$ J·K^{-1}·mol^{-1}

Fe(OH)$_3$(2l) (2L-ferrihydrite)

The solubility product of 2L-ferrihydrite (298.15 K) was selected in TDB 2020 and was complemented with estimates for the enthalpy and heat capacity from Lemire et al. (2013). This leads to the following properties of reaction:

$$Fe(OH)_3(2l) + 3\ H^+ = Fe^{3+} + 3\ H_2O(l) \qquad 2\text{-}11$$

$\log_{10}K_{s,0}°(298.15\ K) = \mathbf{3.5 \pm 0.4}$

$\Delta_r H_m°(298.15\ K) = \mathbf{-(80.846 \pm 2.23)}$ kJ·mol^{-1}

$\Delta_r C_{p,m}°(298.15\ K) = \mathbf{-(35.18 \pm 20.3)}$ J·K^{1}·mol^{-1}

$Mg(OH)_2$(cr) Brucite

The solubility product of brucite was selected in TDB 2020 based on the review of Brown and Ekberg (2016) and was complemented in this update with the selected data for $\Delta_f S_m°$, and $\Delta_f C_{p,m}°$ from Lemire et al. (2013), which are in close agreement with values from Robie and Hemingway (1995). The resulting properties reproduce well the solubility data (Figure 2-7)

$$Mg(OH)_2(s) + 2\ H^+ \rightleftharpoons Mg^{2+} + 2\ H_2O(l) \qquad 2\text{-}12$$

$\log_{10} K_{s,0}°(298.15\ K) = \mathbf{17.11 \pm 0.2}$

$\Delta_r H_m°(298.15\ K) = \mathbf{-(924.45 \pm 0.3)}$ kJ·mol^{-1}

$\Delta_r C_{p,m}°(298.15\ K) = \mathbf{76.9 \pm 0.3}$ J·K^{1}·mol^{-1}

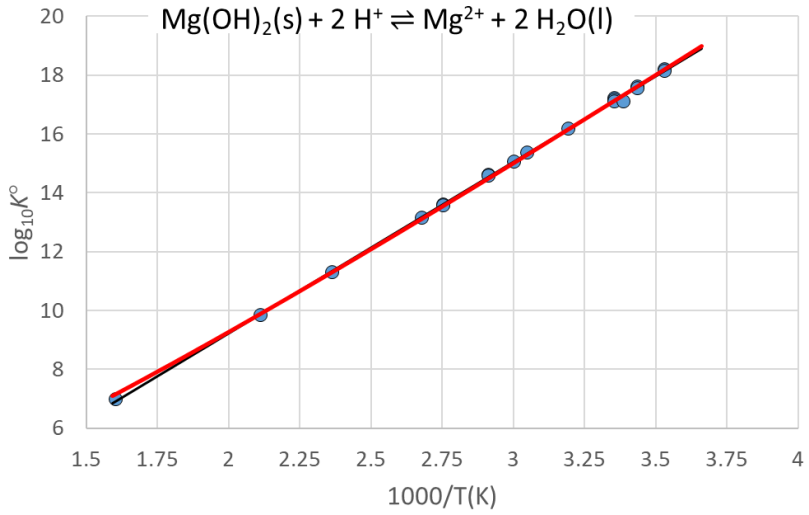

Figure 2-7: Brucite solubility. Blue points are experimental data compiled in (Brown and Ekberg, 2016); black line is TDB 2020; red line is selected properties.

Update for other solids

Thermodynamic properties for the following minerals were updated from previous TDB2020 selection based on the evaluation of Rand et al. (2024), and complemented with molar volumes from Robie and Hemingway (1995).

$CaCO_3$(cr) Calcite

$CaMg(CO_3)_2$(cr) Dolomite

$MgCO_3$(cr) Magnesite

$CaSO_4$2H2O(s) Gypsum

$CaSO_4$(s) Anhydrite

The transition temperature between gypsum and anhydrite based on the selected thermodynamic properties for these phases is estimated to be ~41 ℃, in agreement with experimental data evaluations (Li et al., 2018; Voigt and Freyer, 2023).

$Ca(OH)_2$(cr) Portlandite

SiO_2(am) Amorphous silica

Additional thermodynamic data for wollastonite not selected previously but which are relevant for estimation of missing data of calcium silicates solids and aqueous species were selected based on calorimetry and phase equilibria data. The enthalpy of wollastonite was calculated from the reaction enthalpy:

$$\text{calcite} + \text{quartz} = \text{wollastonite} + CO_2(g) \qquad 2\text{-}13$$

Table 2-1 Values for $\Delta_r H_m°$(298.15 K) for reaction 2-13

Reference	**method**	**$\Delta_r H_m°$(298.15 K) kJ·mol^{-1}**
Charlu et al. (1978)	high temperature oxide melt calorimetry	90.7* ± 0.4
Berman (1988)	phase equilibrium	92.5 ± 0.5**
Chai and Navrotsky (1993)	high temperature solution calorimetry	92.3 ± 1.0
Zhu et al. (1994)	phase equilibrium, high temperature solution calorimetry	89.5* ± 0.2
Robie and Hemingway (1995)	phase equilibrium	89.8 ± 1.4**
Gottschalk (1997)	phase equilibrium	91.2 ± 0.6**
Holland and Powell (2011)	phase equilibrium	91.3 ± 0.5**
	weighted average	**90.3 ± 1.3**

*converted to reaction 2-13 from the formation from oxides, quartz data selected in TDB 2020 and CaO(cr) from Rand et al. (2024); ** uncertainty is that reported for the $\Delta_f H_m°$ wollastonite

Based on the weighted average of the data in literature for reaction 2-13, Table 2-1 and the TDB 2020 data for calcite, quartz and CO_2(g) a value of **-1634.4 ± 1.4** kJ·mol^{-1} for the enthalpy of formation of wollastonite is obtained. The entropy and heat capacity of wollastonite are taken from Robie and Hemingway (1995), to be **81.7 ± 0.1** and **86.2 ± 0.1** J·K^{1}·mol^{-1}, respectively.

$CaSO_4 0.5H_2O$(s) Hemihydrate

Hemihydrate properties were not selected in the TDB2020. This phase is metastable with respect to gypsum and anhydrite and is relevant in industrial and material related processes. The selected thermodynamic properties of this phase are linked to those of gypsum, and are based on the values for the gypsum to hemihydrate reaction retrieved from the evaluation of Li et al. (2018)

$$CaSO_4w2 = CaSO_4w0.5 + 1.5H_2O \qquad 2\text{-}14$$

$$\log_{10}K_{s,0}°(298.15\ K) = \mathbf{-(0.735 \pm 0.35)}$$

$$\Delta_r H_m°(298.15\ K) = \mathbf{18.011 \pm 2)}\ kJ{\cdot}mol^{-1}$$

$$\Delta_r C_{p,m}°(298.15\ K) = \mathbf{47.497 \pm 5}\ J{\cdot}K^{1}{\cdot}mol^{-1}$$

3 Selection for aqueous species

With the exception of data selected in Miron (2024a) for master species, the majority of data for aqueous complexes in the system Fe, Al, Si, Ca, SO_4^{2-}, CO_3^{2-} selected in TDB2020 were left unchanged. These are defined as reactions with properties retrieved from temperature dependent measurements.

Aluminium

The properties of aluminum hydrolysis reactions are left as selected in TDB 2020 (Hummel and Thoenen, 2023) also based on the review of (Brown and Ekberg, 2016), with the exception of $Al(OH)_4^-$ for which the data up to 200 ℃ from (Brown and Ekberg, 2016) were refitted using a two term extrapolation. The plot of $\log_{10}K°$ vs. 1/T(K) shows a linear dependency up to 200 ℃ (Figure 3-1).

$$Al^{3+} + 4H_2O \rightleftharpoons Al(OH)_4^- + 4H^+ \qquad 3\text{-}1$$

$\log_{10}K°(T)$ = **8.74 ±0.2 – 9424 ±67 *IT***

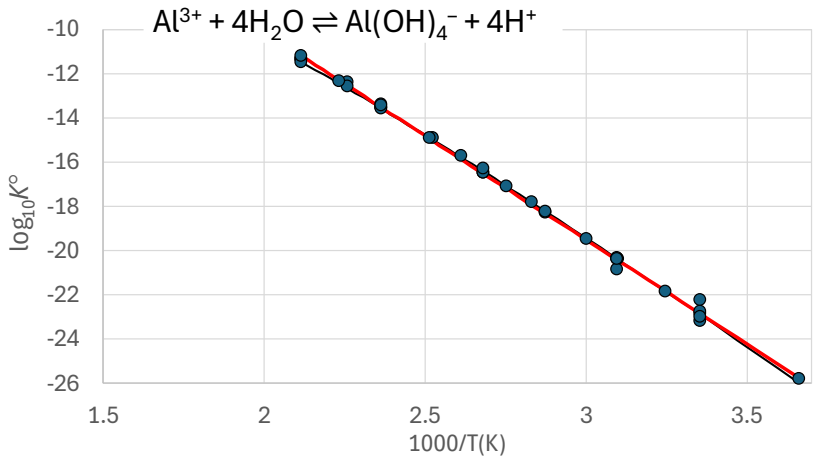

Figure 3-1: Fourth aluminum hydrolysis reaction. Blue points are experimental data compiled in (Brown and Ekberg, 2016); black line uses data in TDB 2020; red line is selected properties.

Iron

The thermodynamic properties of aqueous iron ions (Fe^{3+} and Fe^{2+}) were accepted as selected in TDB 2020 (Hummel and Thoenen, 2023) based on the review of (Lemire et al., 2013) and complemented with the selected $V_m°$ and $C_{p,m}°$ values based on apparent molar heat capacity and molar volume of electrolyte solutions in Miron (2024a).

$$Fe^{3+} + 0.5H_2 = Fe^{2+} + H^+ \qquad 3\text{-}2$$

$$\log_{10}K°(298.15\ K) = \mathbf{13.051 \pm 0.16}$$

$$\Delta_r H_m°(298.15\ K) = \mathbf{-(40.24 \pm 1.7)}\ kJ{\cdot}mol^{-1}$$

$$\Delta_r C_{p,m}°(298.15\ K) = \mathbf{70.6 \pm 10}\ J{\cdot}K^{1}{\cdot}mol^{-1}$$

The ferric-ferrous reaction is in agreement with data from (Tagirov et al., 2000) based on accurate standard potential measurements (Figure 3-2).

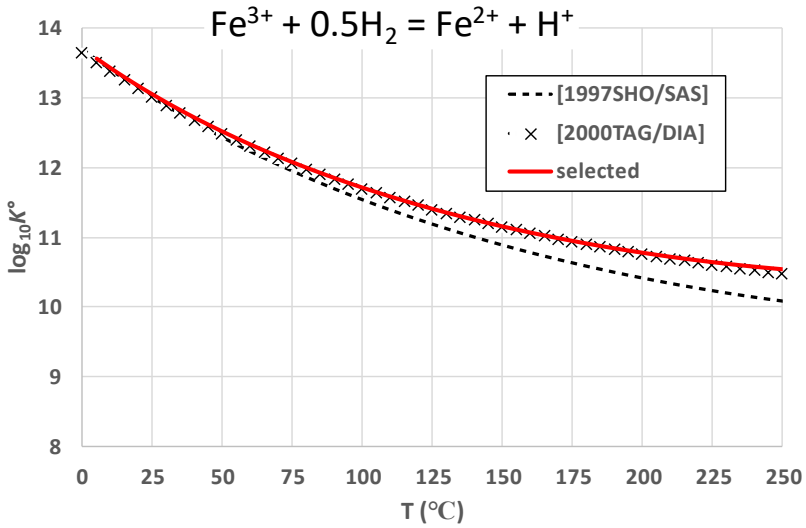

Figure 3-2: $\log_{10}K°(T)$ of the ferric-ferrous reaction calculated based on selected data, compared with the model from (Shock et al., 1997) and (Tagirov et al., 2000).

The properties of ferric and ferrous iron hydrolysis reactions are left as selected in TDB 2020 (Hummel and Thoenen, 2023), also based on the review of (Brown and Ekberg, 2016). For second ferric iron hydrolysis species $Fe(OH)_2^+$ (formation reaction 3-3), no $\Delta_r H_m°$ and $\Delta_r C_{p,m}°$ values were selected in that work.

$$Fe^{3+} + 2\ H_2O(l) = Fe(OH)_2^+ + 2\ H^+ \qquad 3\text{-}3$$

These properties are needed for a complete definition of the temperature dependency of the hydrolysis. The value of $\Delta_r C_{p,m}°$ can be approximated to be equal to zero as seen to be the case in many other isoelectric reactions of this type (e.g., ferrous iron and aluminum hydrolysis). The second hydrolysis reaction for ferrous iron and that of aluminum have values for $\Delta_r H_m°$ which are relatively close, of 115.4 and 110.8 kJ·mol^{-1} respectively, with an average value of 113.1 kJ·mol^{-1}. Assuming a similar temperature dependency for reaction 3-3, the average value is selected as supplemental data.

$$\log_{10}K_s°(298.15\ K) = \mathbf{-(5.71 \pm 0.1)}$$

$$\Delta_r H_m°(298.15\ K) = \mathbf{\textit{-(113.1 \pm 3)}}\ kJ·mol^{-1}$$

$$\Delta_r C_{p,m}°(298.15\ K) = \mathbf{\textit{0}}\ J·K^{1}·mol^{-1}$$

Solubility in the CO_2-H_2O system

Thermodynamic data for the CO_2-H_2O system in the PSI/Nagra database were initially selected in Pearson et al. (1992) from Plummer and Busenberg (1982). For the temperature update in Miron (2024a), the standard thermodynamic properties of HCO_3^- and CO_3^{2-} where updated and made consistent with the HKF model, and values for the heat capacity were selected based on measurements in electrolyte solutions. This update lead to values for the $\Delta_r C_{p,m}°$ that are 55 and 45 J·K^{1}·mol^{-1} more positive for the first and second dissociation reactions, respectively, while maintaining good agreement with experimentally derived $\log_{10}K°$ data. The difference in $\Delta_r C_{p,m}°$ comes from the difference in the values for the heat

capacity of individual species used to calculated the values for the reaction in the past selection of data.

Selected properties describing the solubility of $CO_{2(g)}$ in water, forming the $CO_{2(aq)}$ complex, are:

$$CO_{2(g)} = CO_{2(aq)} \qquad 3\text{-}4$$

$$\log_{10}K°(298.15\ K) = \mathbf{-(1.47 \pm 0.05)}$$

$$\Delta_r H_m°(298.15\ K) = \mathbf{-(19.7 \pm 0.3)}\ kJ{\cdot}mol^{-1}$$

$$\Delta_r C_{p,m}°(298.15\ K) = \mathbf{153 \pm 10}\ J{\cdot}K^{1}{\cdot}mol^{-1}$$

Compared with the previous selection in (Pearson et al., 1992) where $\Delta_r C_{p,m}° = 208\ J{\cdot}K^{1}{\cdot}mol^{-1}$.

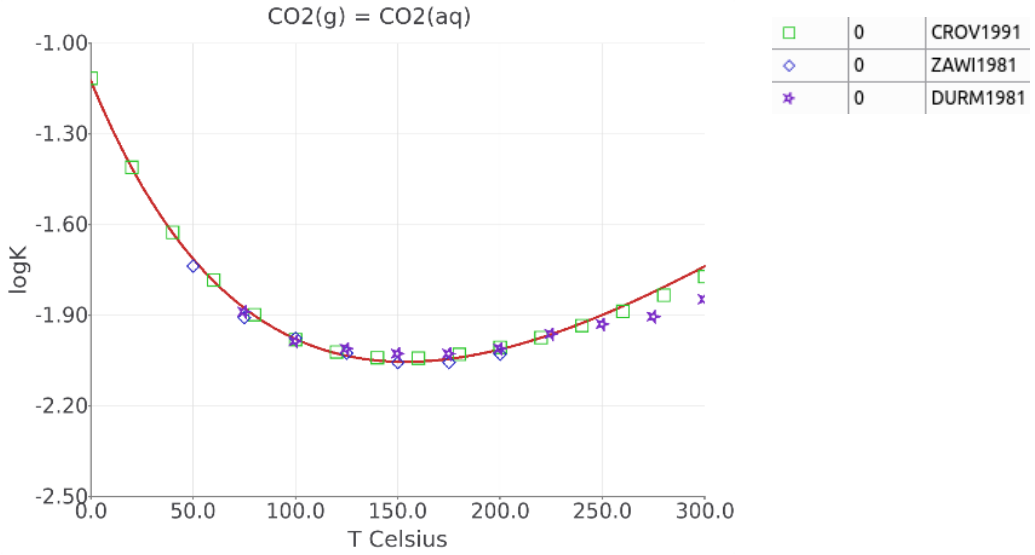

Figure 3-3: Carbon dioxide solubility in water as a function of temperature; measured data (Crovetto, 1991; Drummond, 1981; Zawisza and Malesinska, 1981) compared with calculated values based on the selected thermodynamic data (red line).

Selected data for the 1st dissociation reaction

$$CO_{2(aq)} + H_2O(l) = H^+ + HCO_3^- \qquad 3\text{-}5$$

$$\log_{10}K°(298.15\ K) = \mathbf{-(6.352 \pm 0.05)}$$

$$\Delta_r H_m°(298.15\ K) = \mathbf{-(9.1 \pm 0.3)}\ kJ{\cdot}mol^{-1}$$

$$\Delta_r C_{p,m}°(298.15\ K) = \mathbf{-(311 \pm 10)}\ J{\cdot}K^{1}{\cdot}mol^{-1}$$

This can be compared with the previous selection in Pearson et al. (1992) where $\Delta_r C_{p,m}^\circ$ = -366 J·K[1]·mol^{-1} (Figure 3-4).

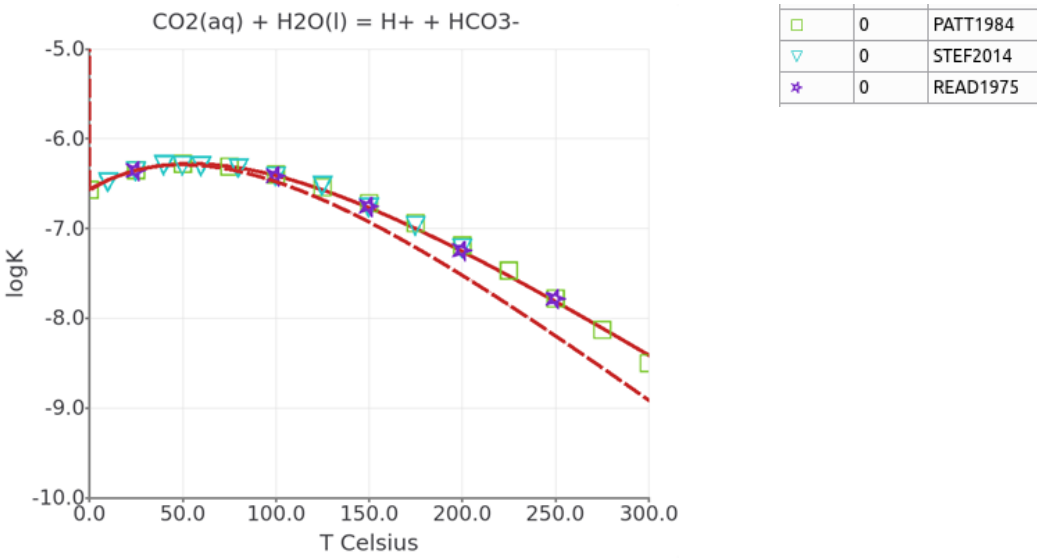

Figure 3-4: First dissociation of dissolved carbon dioxide as a function of temperature, measured data (Patterson et al., 1982; Read, 1975; Stefánsson et al., 2014) compared with calculated values based on the selected thermodynamic data (red line) and selection in Pearson et al. (1992) (dashed red line).

The properties of the bicarbonate/carbonate reaction are calculated based on the selection in Miron (2024a) for the standard properties of individual species.

$$HCO_3^- = H^+ + CO_3^{2-} \qquad 3\text{-}6$$

$$\log_{10}K^\circ(298.15\ \text{K}) = \mathbf{-(10.329 \pm 0.1)}$$

$$\Delta_r H_m^\circ(298.15\ \text{K}) = \mathbf{14.7 \pm 0.6}\ \text{kJ·mol}^{-1}$$

$$\Delta_r C_{p,m}^\circ(298.15\ \text{K}) = \mathbf{-(245 \pm 10)}\ \text{J·K}^{1}\text{·mol}^{-1}$$

This can be compared with the previous selection in (Pearson et al., 1992) where $\Delta_r C_{p,m}^\circ$ = -290 J·K[1]·mol^{-1} (Figure 3-5).

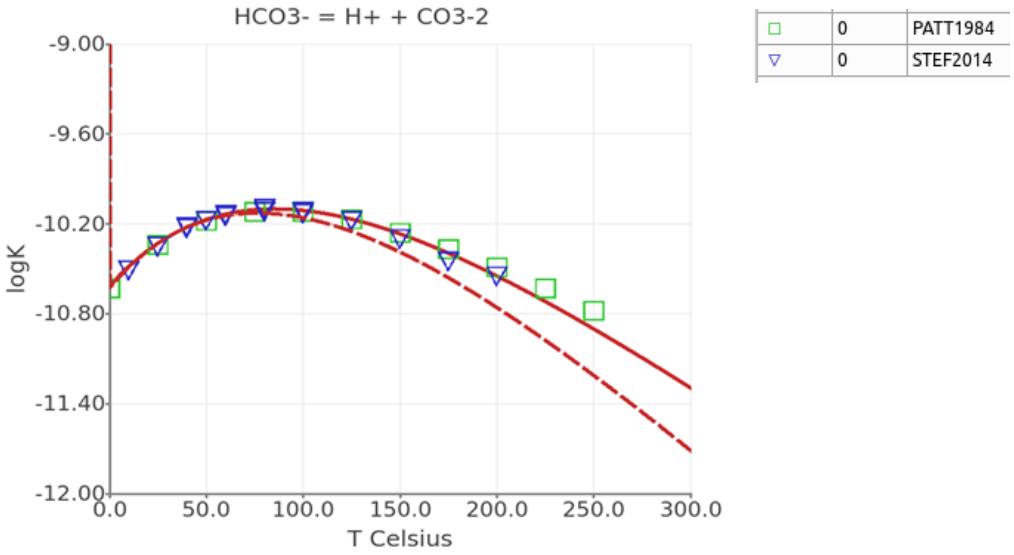

Figure 3-5: Bicarbonate/carbonate equilibria as a function of temperature; measured data (Patterson et al., 1984; Stefánsson et al., 2014) compared with calculated values based on the selected thermodynamic data using a 3-term extrapolation method (Miron et al., 2020) (red line) and selection in Pearson et al. (1992) (dashed red line).

Heat capacity and molar volume for phosphate aqueous species

Thermodynamic properties concerning the temperature dependence of the second and third hydrolysed species of the phosphoric acid were selected in Miron (2024a). Here heat capacity and molar volume values are selected for the $H_2PO_4^-$ and H_3PO_4(aq) species based on aqueous electrolyte measurements. These data are relevant for phosphate systems and estimating missing temperature data by writing isocoulombic and isoelectric reactions (Miron et al., 2020).

H_3PO_4(aq)

Electrolyte data:

$V_m°(H_3PO_4(aq), 298.15\ K) = 48.1\ cm^3\ mol^{-1}$ (Larson et al., 1982)

$V_m°(H_3PO_4(aq), 298.15\ K) = 47.8\ cm^3\ mol^{-1}$ (Ballerat-Busserolles et al., 2007)

$C_{p,m}°(H_3PO_4(aq), 298.15\ K) = 94\ J{\cdot}K^{-1}{\cdot}mol^{-1}$ (Larson et al., 1982)

$C_{p,m}°(H_3PO_4(aq), 298.15\ K) = 98\ J{\cdot}K^{-1}{\cdot}mol^{-1}$ (Ballerat-Busserolles et al., 2007)

Selected average values:

$V_m°(H_3PO_4(aq), 298.15\ K) =$ **48** $cm^3\ mol^{-1}$

$C_{p,m}°(H_3PO_4(aq), 298.15\ K)$ = **96** $J·K^{-1}·mol^{-1}$

$H_2PO_4^-$

Electrolyte data:

$V_m°(NaH_2PO_4(aq), 298.15\ K) = 30.1\ cm^3\ mol^{-1}$ (Larson et al., 1982)

$V_m°(NaH_2PO_4(aq), 298.15\ K) = 7\ cm^3\ mol^{-1}$ (Ballerat-Busserolles et al., 2007)

$C_{p,m}°(NaH_2PO_4(aq), 298.15\ K) = 9\ J·K^{-1}·mol^{-1}$ (Larson et al., 1982)

$C_{p,m}°(NaH_2PO_4(aq), 298.15\ K) = 30\ J·K^{-1}·mol^{-1}$ (Ballerat-Busserolles et al., 2007)

From the average values and using Eq. 3-2 in Miron (2024a) and properties of Na^+, the selected values are obtained:

$V_m°(H_2PO_4^-, 298.15\ K)$ = **31** $cm^3\ mol^{-1}$

$C_{p,m}°(H_2PO_4^-, 298.15\ K)$ = **-31** $J·K^{-1}·mol^{-1}$

Updated thermodynamic data for $CaSiO_2(OH)_2$(aq)

This neutral calcium silica aqueous species is suggested to control the amount of dissolved silicon in equilibrium with calcium silicate hydrates at high pH and Ca/Si ratio. The data from this species was selected based on the potentiometric titrations of Santschi and Schindler (1974)

$$Ca^{2+} + SiO_2(OH)_2^{2-} = CaSiO_2(OH)_2(aq) \qquad 3\text{-}7$$

$$\log_{10}K°(298.15\ K) = 4.5 \pm 0.15$$

Nicoleau and Schreiner (2017) determined the $\log_{10}K°(298.15\ K)$ to be 2.9. To improve the agreement between the modeled and measured C-S-H (Calcium Silicate Hydrate) Si solubility using different solid models Walker et al. (2016) and Kulik et al. (2022) arrived to a value for $\log_{10}K°(298.15\ K)$ of 4. In order to maintain the consistency with the cement model this value is selected. For the temperature stability of this species the entropy and heat capacities are derived from the isocoulombic reaction of wollastonite solubility and are therefore assumed to be equal to those of wollastonite (as well as the molar volume).

The selected data for reaction 3-7 are:

$$\log_{10}K°(298.15\ K) = \mathbf{4.0 \pm 0.5}$$

$$\Delta_r S_{,m}°(298.15\ K) = \mathbf{288.31 \pm 0.5}\ J·K^{1}·mol^{-1}$$

$$\Delta_r C_{p,m}°(298.15\ K) = \mathbf{422.98 \pm 0.5}\ J·K^{1}·mol^{-1}$$

Table 3-1 Selected temperature coefficients for heat capacities in this work according to the formula: $C_{p,m}° = a_0 + a_1 \cdot T + a_2 \cdot T^{-2} + a_3 \cdot T^{-0.5} + a_4 \cdot T^2 + a_8 \cdot T^{-1}$, where T is the temperature (K), not available in previous TDB releases.

name	**formula**	**$C_{p,m}°$[a] J·K⁻¹·mol⁻¹**	**a_0**	**a_1**	**a_2**	**a_3**	**a_4**	**a_8**	**T min (K)**	**T max (K)**
Quartz[b]	SiO_2	44.586	8.1145E+01	1.8280E-02	-1.8100E+05	-6.9850E+02	5.4060E-06		298	847
Corundum[b]	Al_2O_3	79.095	1.6120E+02	-1.3520E-03	-1.8150E+06	-1.0590E+03	5.3810E-07		298	1000
Gibbsite[b]	$Al(OH)_3$	91.719	5.4700E+01	1.7027E-01	-1.2220E+06					
Hematite[b]	Fe_2O_3	104.029	1.5015E+03	-1.2146E+00	1.4123E+07	-2.1493E+04	5.6900E-04		298	950
Magnetite[b]	Fe_3O_4	150.864	2.6591E+03	-2.5215E+00	2.0734E+07	-3.6455E+04	1.3677E-03		298	800
Goethite[c]	FeOOH	74.319	8.0361E+01	-8.7560E-02	-5.9408E+05		3.7689E-04	-2.0142E+03	200	373
Lepidocrocite[c]	FeOOH	69.135	9.0981E+01	4.3899E-02	3.8679E+05		-2.9818E-05	-1.09E+04	200	387
Portlandite[d]	$Ca(OH)_2$	87.488	8.9264E+01	3.3112E-02	-1.0355E+06				298	700
Brucite[d]	$Mg(OH)_2$	76.883	9.3393E+01	3.0121E-02	-2.2659E+06				298	600
Calcite[d]	$CaCO_3$	83.472	7.8781E+01	5.6868E-02	-1.0902E+06				298	1200
Dolomite	$CaMg(CO_3)_2$	157.510	8.2795E+01	3.4800E-01	-9.7121E+05		-2.0378E-04		298	650
Magnesite	$MgCO_3$	76.108	7.3335E+01	6.3990E-02	-1.4495E+06				298	800
Anhydrite	$CaSO_4$	101.224	3.7280E+02	-1.5740E-01	1.6950E+06	-4.3308E+03	7.9900E-05		298	1000
Wollastonite	$CaSiO_3$	86.193	2.0078E+02	-2.5890E-02	-1.5790E+05	-1.8260E+03	7.4340E-06		298	1400

[a] calculated with $C_{p,m}°$ temperature function for T = 298.15 K, [b] Robie and Hemingway (1995), [c] Lemire et al.(2013), [d] Rand et al. (2024)

4 References

Apps, J.A., Neil, J.M. & Jun, C.H. (1989): Thermochemical properties of gibbsite, bayerite, boehmite, diaspore, and the aluminate ion between 0 and 350 C. Division of Waste Management, Office of Nuclear Material Safety and Safeguard, US NRC NUREG/CR-5271-LBL-21482. Berkeley, CA. https://doi.org/10.2172/6481805

Ballerat-Busserolles, K., Sedlbauer, J. & Majer, V. (2007): Standard Thermodynamic Properties of H 3 PO 4 (aq) over a Wide Range of Temperatures and Pressures. https://doi.org/10.1021/jp064650m

Bénézeth, P., Palmer, D.A. & Wesolowski, D.J. (2001): Aqueous high-temperature solubility studies. II. The solubility of boehmite at 0.03 m ionic strength as a function of temperature and pH as determined by in situ measurements. *Geochimica et Cosmochimica Acta* 65, 2097–2111. https://doi.org/10.1016/S0016-7037(01)00585-3

Berman, R.G. (1988): Internally-consistent thermodynamic data for minerals in the system Na2O-k2O-CaO-MgO-FEO-Fe2O3-Al2O3-SiO2-TiO2-H2O-CO2. *Journal of Petrology* 29, 445–522. https://doi.org/10.1093/petrology/29.2.445

Brown, P.L. & Ekberg, C. (2016): Hydrolysis of metal ions at 25°C. Wiley-VCH Verlag GmbH & Co., Weinheim, Germany.

Chai, L. & Navrotsky, A. (1993): Thermochemistry of carbonate-pyroxene equilibria. *Contributions to Mineralogy and Petrology* 114, 139–147. https://doi.org/10.1007/BF00307751/METRICS

Charlu, T. V., Newton, R.C. & Kleppa, O.J. (1978): Enthalpy of formation of some lime silicates by high-temperature solution calorimetry, with discussion of high pressure phase equilibria. *Geochimica et Cosmochimica Acta* 42, 367–375. https://doi.org/10.1016/0016-7037(78)90267-3

Chen, B., Xu, X., Chen, X., Kong, L. & Chen, D. (2018): Transformation behavior of gibbsite to boehmite by steam-assisted synthesis. *Journal of Solid State Chemistry* 265, 237–243. https://doi.org/10.1016/J.JSSC.2018.06.010

Chen, Q. & Zeng, W. (1996): Calorimetric determination of the standard enthalpies of formation of gibbsite, Al(OH)3(cr), and boehmite, AlOOH(cr). *Geochimica et Cosmochimica Acta* 60, 1–5. https://doi.org/10.1016/0016-7037(95)00378-9

Chesworth, W. (1972): The stability of gibbsite and boehmite at the surface of the earth. *Clays and Clay Minerals* 20, 369–374. https://doi.org/10.1346/CCMN.1972.0200604

Cox, J.D., Wagman, D.D. & Medvedev, V.A. (Vadim A. (1989): *CODATA key values for thermodynamics*. Hemisphere Pub. Corp, New York.

Crovetto, R. (1991): Evaluation of solubility data of the system CO2–H2O from 273 K to the critical point of water. *Journal of Physical and Chemical Reference Data* 20, 575–589. https://doi.org/10.1063/1.555905

Drummond, S. (1981): Boiling and mixing of hydrothermal fluids: chemical effects on mineral precipitation.

Glasser, L. & Jenkins, H.D.B. (2016): Predictive thermodynamics for ionic solids and liquids. *Physical Chemistry Chemical Physics* 18, 21226–21240. https://doi.org/10.1039/c6cp00235h

Gottschalk, M. (1997): Internally consistent thermodynamic data for rock-forming minerals in the system SiO2-TiO2-Al2O3-CaO-MgO-FeO-K2O-Na2O-H2O-CO2. *European Journal of Mineralogy* 9, 175–223.

Guggenheim, E.A. & Turgeon, J.C. (1955): Specific interaction of ions. *Transactions of the Faraday Society* 51, 747–761. https://doi.org/10.1039/TF9555100747

Hemingway, B.S. & Robie, R.A. (1977): Enthalpies of formation of low albite (NaAlSi3O8), gibbsite (Al(OH)3), and NaAlO2; revised values for ΔH°f,298 and ΔG°f,298 of some aluminosilicate minerals. *J Res US Geol Surv* 5, 413–429.

Hemingway, B.S., Robie, R.A. & Apps, J.A. (1991): Revised values for the thermodynamic properties of boehmite, AlO(OH) , and related species and phases in the system Al-H-O. *American Mineralogist* 76, 445–457.

Hemingway, B.S., Robie, R.A., Fisher, J.R. & Wilson, W.H. (1977): Heat capacities of gibbsite, Al(OH)3, between 13 and 480 K and magnesite, MgCO3, between 13 and 380 K and their standard entropies at 289. 15 K, and the heat capacities of calorimetry conference benzoic acid between 12 and 316 K. *J Res US Geol Surv* 5, 797–806.

Holland, T.J.B. & Powell, R. (2011): An improved and extended internally consistent thermodynamic dataset for phases of petrological interest, involving a new equation of state for solids. *Journal of Metamorphic Geology* 29, 333–383.

Hsu, P.H. (1989): Aluminum hydroxides and oxyhydroxides, in: Minerals in Soil Environments. wiley, pp. 331–378. https://doi.org/10.2136/sssabookser1.2ed.c7

Hummel, W., Berner, U., Curti, E., Pearson, F.J. & Thoenen, T. (2002): Nagra/PSI Chemical Thermodynamic Data Base 01/01. *Radiochimica Acta* 90, 805–813. https://doi.org/10.1524/ract.2002.90.9-11_2002.805

Hummel, W. & Thoenen, T. (2023): The PSI Chemical Thermodynamic Database 2020. Nagra Technical Report, NTB 21-03.

Kulik, D.A., Miron, G.D. & Lothenbach, B. (2022): A structurally-consistent CASH+ sublattice solid solution model for fully hydrated C-S-H phases: Thermodynamic basis, methods, and Ca-Si-H2O core sub-model. *Cement and Concrete Research* 151, 106585. https://doi.org/10.1016/j.cemconres.2021.106585

Kulik, D.A., Wagner, T., Dmytrieva, S. V., Kosakowski, G., Hingerl, F.F., Chudnenko, K. V. & Berner, U.R. (2013): GEM-Selektor geochemical modeling package: Revised algorithm and GEMS3K numerical kernel for coupled simulation codes. *Computational Geosciences* 17, 1–24. https://doi.org/10.1007/s10596-012-9310-6

Larson, J.W., Zeeb, K.G. & Hepler, L.G. (1982): Heat capacities and volumes of dissociation of phosphoric acid (1st, 2nd, and 3rd), bicarbonate ion, and bisulfate ion in aqueous solution. *Canadian Journal of Chemistry* 60, 2141–2150. https://doi.org/10.1139/v82-306

Lemire, R.J., Berner, U., Musikas, C., Palmer, D.A., Taylor, P. & Tochiyama, O. (2013): Chemical thermodynamics of iron Part 1. *Chemical thermodynamics* 13a, 1–1082. https://doi.org/NEA No. 6355

Li, D., Zeng, D., Yin, X. & Gao, D. (2018): Phase diagrams and thermochemical modeling of salt lake brine systems. III. Li2SO4+H2O, Na2SO4+H2O, K2SO4+H2O, MgSO4+H2O and CaSO4+H2O systems. *Calphad* 60, 163–176. https://doi.org/10.1016/J.CALPHAD.2018.01.002

Lothenbach, B., Geiger, C.A., Dachs, E., Winnefeld, F. & Pisch, A. (2022): Thermodynamic properties and hydration behavior of ye'elimite. *Cement and Concrete Research* 162, 106995. https://doi.org/10.1016/J.CEMCONRES.2022.106995

Lothenbach, B., Pelletier-Chaignat, L. & Winnefeld, F. (2012): Stability in the system CaO-Al2O3-H2O. *Cement and Concrete Research* 42, 1621–1634. https://doi.org/10.1016/j.cemconres.2012.09.002

Majzlan, J., Navrotsky, A. & Casey, W.H. (2000): Surface Enthalpy of Boehmite. *Clays and Clay Minerals* 48, 699–707. https://doi.org/10.1346/CCMN.2000.0480611

Miron, G.D. (2024a): PSI/Nagra TDB, effect of temperature and pressure: I. Selection of molar volumes for solid phases and T-P dependency for master and selected aqueous species. TM-44-24-03. Villigen PSI.

Miron, G.D. (2024b): Si–Al Pitzer dataset: Consistent set of Pitzer activity model interaction parameters of Al and Si species, for modelling cements in saline systems with THEREDA. https://doi.org/10.26434/CHEMRXIV-2024-M02F1-V2

Miron, G.D., Kulik, D.A. & Thoenen, T. (2020): Generating isocoulombic reactions as a tool for systematic evaluation of temperature trends of thermodynamic properties: Application to aquocomplexes of lanthanides and actinides. *Geochimica et Cosmochimica Acta* 286, 119–142. https://doi.org/10.1016/j.gca.2020.07.020

Navrotsky, A., Mazeina, L. & Majzlan, J. (2008): Size-driven structural and thermodynamic complexity in iron oxides. *Science*. https://doi.org/10.1126/science.1148614

Nicoleau, L. & Schreiner, E. (2017): Determination of Ca2+ complexation constants by monomeric silicate species at 25 °C with a Ca2+ ion selective electrode. *Cement and Concrete Research* 98, 36–43. https://doi.org/10.1016/j.cemconres.2016.12.007

Palmer, D.A. & Wesolowski, D.J. (1992): Aluminum speciation and equilibria in aqueous solution: II. The solubility of gibbsite in acidic sodium chloride solutions from 30 to 70°C. *Geochimica et Cosmochimica Acta* 56, 1093–1111. https://doi.org/10.1016/0016-7037(92)90048-N

Panasyuk, G.P., Belan, V.N., Voroshilov, I.L. & Kozerozhets, I. V. (2010): Hydrargillite → boehmite transformation. *Inorganic Materials 2010 46:7* 46, 747–753. https://doi.org/10.1134/S0020168510070113

Patterson, C.S., Busey, R.H. & Mesmer, R.E. (1984): Second ionization of carbonic acid in NaCl media to 250°C. *Journal of Solution Chemistry* 13, 647–661. https://doi.org/10.1007/BF00650372

Patterson, C.S., Slocum, G.H., Busey, R.H. & Mesmer, R.E. (1982): Carbonate equilibria in hydrothermal systems: First ionization of carbonic acid in NaCl media to 300°C. *Geochimica et Cosmochimica Acta* 46, 1653–1663. https://doi.org/10.1016/0016-7037(82)90320-9

Pearson, F.J., Berner, U. & Hummel, W. (1992): Nagra Thermochemical Data Base II. Supplemental Data 05/92. Nagra Technical Report NTB 91-18. Wettingen, Switzerland.

Peryea, F.J. & Kittrick, J.A. (1988): Relative solubility of corundum, gibbsite, boehmite, and diaspore at standard state conditions. *Clays & Clay Minerals* 36, 391–396. https://doi.org/10.1346/ccmn.1988.0360502

Plummer, L.N. & Busenberg, E. (1982): The solubilities of calcite, aragonite and vaterite in

CO2-H2O solutions between 0 and 90°C, and an evaluation of the aqueous model for the system CaCO3-CO2-H2O. *Geochimica et Cosmochimica Acta* 46, 1011–1040. https://doi.org/10.1016/0016-7037(82)90056-4

Rand, M.H., Palmer, D.A., Fuger, J. & Gajda, T. (2024): *Selected ancillary compounds of interest to radioactive waste management. Chemical Thermodynamics volume 15. NEA TDB*.

Read, A.J. (1975): The first Ionization constant of carbonic acid from 25 to 250°C and to 2000 bar. *Journal of Solution Chemistry* 4, 53–70. https://doi.org/10.1007/BF00646052

Robie, R. & Hemingway, B.S. (1995): Thermodynamic Properties of Minerals and Related Substances at 298.15K and 1 Bar, U.S. Geological Survey Bulletin.

Russell, A.S., Edwards, J.D. & Taylor, C.S. (1955): Solubility and Density of Hydrated Aluminas in NaOH Solutions. *JOM* 7, 1123–1128. https://doi.org/10.1007/bf03377627

Santschi, P.H. & Schindler, P.W. (1974): Complex formation in the ternary systems CaII–H4SiO4–H2O and MgII–H4SiO4–H2O. *J. Chem. Soc., Dalton Trans.* 181–184. https://doi.org/10.1039/DT9740000181

Shin, G.H., Park, C.W., Kang, J.H., Seo, S.Y., Tran, T. & Kim, M.J. (2020): Study on precipitation of microcrystalline boehmite from bayer process solutions. *Journal of Ceramic Processing Research* 21, 50–56. https://doi.org/10.36410/JCPR.2020.21.1.50

Shock, E.L., Sassani, D.C., Willis, M. & Sverjensky, D.A. (1997): Inorganic species in geologic fluids: Correlations among standard molal thermodynamic properties of aqueous ions and hydroxide complexes. *Geochimica et Cosmochimica Acta* 61, 907–950. https://doi.org/10.1016/S0016-7037(96)00339-0

Skoufadis, C., Panias, D. & Paspaliaris, I. (2003): Kinetics of boehmite precipitation from supersaturated sodium aluminate solutions. *Hydrometallurgy* 68, 57–68. https://doi.org/10.1016/S0304-386X(02)00165-2

Stefánsson, A., Bénézeth, P. & Schott, J. (2014): Potentiometric and spectrophotometric study of the stability of magnesium carbonate and bicarbonate ion pairs to 150 °C and aqueous inorganic carbon speciation and magnesite solubility. *Geochimica et Cosmochimica Acta* 138, 21–31. https://doi.org/10.1016/J.GCA.2014.04.008

Tagirov, B.R., Diakonov, I.I., Devina, O.A. & Zotov, A. V. (2000): Standard ferric-ferrous potential and stability of FeCl2+ to 90°C. Thermodynamic properties of Fe((aq))3+ and ferric-chloride species. *Chemical Geology* 162, 193–219. https://doi.org/10.1016/S0009-2541(99)00150-3

Trolard, F. & Tardy, Y. (1987): The stabilities of gibbsite, boehmite, aluminous goethites and aluminous hematites in bauxites, ferricretes and laterites as a function of water activity, temperature and particle size. *Geochimica et Cosmochimica Acta* 51, 945–957. https://doi.org/10.1016/0016-7037(87)90107-4

Verdes, G., Gout, R. & Castet, S. (1992): Thermodynamic properties of the aluminate ion and of bayerite, boehmite, diaspore and gibbsite. *European Journal of Mineralogy* 4, 767–792. https://doi.org/10.1127/EJM/4/4/0767

Voigt, W. & Freyer, D. (2023): Solubility of anhydrite and gypsum at temperatures below 100°C and the gypsum-anhydrite transition temperature in aqueous solutions: a re-assessment. *Frontiers in Nuclear Engineering* 2, 1208582. https://doi.org/10.3389/FNUEN.2023.1208582/BIBTEX

Walker, C.S., Sutou, S., Oda, C., Mihara, M. & Honda, A. (2016): Calcium silicate hydrate (C-S-H) gel solubility data and a discrete solid phase model at 25 °C based on two binary non-ideal solid solutions. *Cement and Concrete Research* 79, 1–30. https://doi.org/10.1016/j.cemconres.2015.07.006

Wesolowski, D.J. (1992): Aluminum speciation and equilibria in aqueous solution: I. The solubility of gibbsite in the system Na-K-Cl-OH-Al(OH)4 from 0 to 100°C. *Geochimica et Cosmochimica Acta* 56, 1065–1091. https://doi.org/10.1016/0016-7037(92)90047-M

Zawisza, A. & Malesinska, B. (1981): Solubility of Carbon Dioxide in Liquid Water and of Water in Gaseous Carbon Dioxide in the Range 0.2-5 MPa and at Temperatures up to 473 K. *Journal of Chemical and Engineering Data* 26, 388–391. https://doi.org/10.1021/JE00026A012/ASSET/JE00026A012.FP.PNG_V03

Zhang, H., Zhang, X., Graham, T.R., Pearce, C.I., Hlushko, H., Laverne, J.A., Liu, L., Wang, S., Zheng, S., Zhang, Y., Clark, S.B., Li, P., Wang, Z. & Rosso, K.M. (2021): Crystallization and phase transformations of aluminum (oxy)hydroxide polymorphs in caustic aqueous solution. *Inorganic Chemistry* 60, 9820–9832. https://doi.org/10.1021/acs.inorgchem.1c01111

Zhu, H., Newton, R.C. & Kleppa, O.J. (1994): Enthalpy of formation of wollastonite (CaSiO3) and anorthite (CaAl2Si2O8) by experimental phase equilibrium measurements and high-temperature solution colorimetry. *American Mineralogist* 79, 134–144.